JMEPEG (2011) 20:579–583
DOI: 10.1007/s11665-010-9794-y

1059-9495/$19.00

Accelerated Fatigue Testing of Stent-Like Diamond Specimens

A. Zipse, M. Schlun, G. Dreher, J. Zum Gahr, and N. Rebelo

(Submitted May 14, 2010; in revised form November 18, 2010)

In this study, we investigated the fatigue behavior of stent-like diamond specimens with particular attention paid to the nature of the test specimen, the constitutive model for the finite element analyses and the displacement condition. A newly designed test rig did enhance the investigation and results with respect to the simulation of the expected in vivo displacement conditions. The excellent performance of the new test method presented within our study provides a good basis for future tests without risk of compromised results due to differing characteristics between test specimens and finished stents, inappropriate displacement conditions or constitutive material model and provides a high reliability and applicability of the results to actual stents.

Keywords fatigue, nitinol, stents, ε/N curve

1. Introduction

In recent years, many studies on the fatigue behavior of NiTi have been published, such as (Ref 1-3). The complexity of the fatigue behavior of NiTi has increasingly been taken into consideration within these studies, necessitating enhanced test methods, sophisticated test-equipment, improved test specimen, and better constitutive models. In this vein, the goal of this study was to continue building on the work of previous fatigue effect studies in order to obtain accurate data applicable to the fatigue behavior of NiTi stents. The test specimens for this study were processed in a similar manner to conventional NiTi stents and embedded in a stent-like structure. The test rig was designed to achieve a circumferential load onto the struts. Finally, the existing ABAQUS material model for NiTi, used for the determination of the mean strains and strain amplitudes, was enhanced to capture some of the phenomena in the uniaxial behavior of NiTi due to cyclic deformation. In contrast to several previous studies (Ref 2, 3), the test specimen was not a Nitinol wire, but more representative for a conventional laser-cut Nitinol stent with respect to its design and process. Furthermore, in contrast to a more realistic study related to a laser-cut Nitinol stent (Ref 1), the displacements onto the test specimen in this study reflects more accurate the in vivo displacements a stent experiences.

This article is an invited paper selected from presentations at Shape Memory and Superelastic Technologies 2010, held May 16-20, 2010, in Pacific Grove, California, and has been expanded from the original presentation.

A. Zipse, M. Schlun, G. Dreher, and **J. Zum Gahr**, Bard Peripheral Vascular, R&D, Tempe, AZ; and **N. Rebelo**, DS Simulia Corp, SIMULIA Western Region, Fremont, CA. Contact e-mail: achim.zipse@crbard.com.

2. Materials and Methods

The test specimens used in the fatigue tests were embedded into a stent framework in order to allow them to undergo the same standard manufacturing methods as stents, such as laser cutting, heat treatment, and surface finish. The specimens were manufactured from raw material identical to that used for conventional NiTi stents and meeting the requirements of ASTM standard F2633-07. The test specimens then underwent all the same standard manufacturing process steps as the stents, using the same equipment, in order to ensure the material equivalence of the specimens to the stents. The diamond geometry of the study specimens falls within the range of typical stent geometries. Figure 1 shows a stent framework with four stent-like diamond specimens incorporated. Each diamond specimen contains two V-shaped specimens, one on each the left and the right-hand side of the clamping extensions. The individual diamond specimen were cut out from the stent framework at the struts which poke out of the clamping area and are outside the diamond specimen, see Fig. 1 and 3.

The fatigue tests were conducted in a newly developed test rig. Each of the specimen slots could be controlled individually, allowing for the running of different load levels simultaneously. Each slot was equipped with one specimen holder that applied a circumferential load onto the specimen. The specimen holder was powered by a brushless DC motor with a high resolution encoder. Figure 2 shows a picture of the test rig.

Sixteen V-specimens were tested for each of the eight strain levels, resulting in 128 total test specimens. The displacement sequence was as follows (maximum principal strains computed at the most loaded point):

- Displace to ~7.5% pre-strain and subsequent unloading; this represents the loading of the stent into the delivery system.
- Displace to ~2.5% strain (range from 2.4 to 2.55%); this represents the situation after deployment of the stent in a vessel (that always has a smaller diameter than the nominal diameter of the stent applied).

- Fatigue strain amplitudes (0.38, 0.52, 0.57, 0.63, 0.65, 1.15, 1.39, and 1.62%); this represents the strains that the stent struts experience in vivo.

The specimens were tested with a circumferential displacement in a pull condition (displacement via the opening of the diamond specimen) for a maximum of 10^7 cycles. Although a push condition would be the correct test setup for an evaluation of a straight pulsatile condition, either a push or pull condition is appropriate for testing of a curved pulsatile condition or non-radial in vivo deformations. All external loads such as bending, compression or torsion, occurring, for example, in the femoro-popliteal arteries, are provoking the same local deformation of the stent structure. This local deformation is an opening or closing of adjacent strut pairs of a real stent structure. Figure 3 shows the deformation of the diamond specimen in the specimen holder of the test rig.

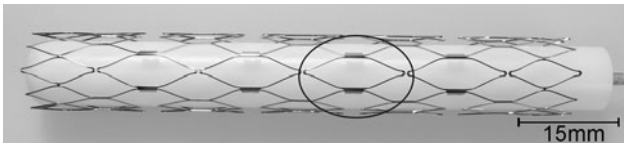

Fig. 1 Diamond test specimen incorporated into stent framework (one diamond specimen example highlighted)

Fig. 2 Test rig with individually controlled specimen holders and motors

Furthermore, there are two locations within the diamond specimen that showed a very similar maximum strain amplitude at a given angle. One location is on the outer side (nearby clamping area) of the specimen and one location on the inside (apex) of the specimen, so that potential differences in surface quality will be captured as well. Since both locations exist two times per V-specimen, there are four potential fracture locations for the V-specimen, so that the chosen configuration of specimen design and test setup represents a conservative approach. The tests were conducted at 37 ± 1 °C in a water bath at 30 Hz.

The finite element analyses have been performed with ABAQUS/Standard 6.9-2 and the strain amplitudes for this study were determined with the help of a newly developed ABAQUS material model, capable of capturing the most relevant effects of the cyclic behavior of NiTi. In order to get accurate results (strain amplitudes) from the given angles, specific attention was paid on the implementation of the material model, boundary conditions, and appropriate mesh density.

Tensile tests on dog-bone specimen have been performed that were processed with identical parameter and equipment such as the diamond specimen for the determination of the material parameter. The boundary conditions reflect the circumferential load onto the specimen and a mesh density study has been performed. For all analyses, 12 three-dimensional, linear elements were used along the strut width and strut thickness and due to symmetry; one quarter of the diamond specimen was used.

3. Results

Figure 4 shows a picture of a specimen after fracture. Fractures occurred both at the apex and adjacent to the clamping area of the diamond specimen. The maximum strain amplitude that resulted at each location at a given angle was very similar throughout the range of strain levels, though the strain amplitude levels were marginally higher at the apex.

Figure 5 shows a SEM picture of the surface of a typical apex fracture. As shown, the crack initiation is located on the

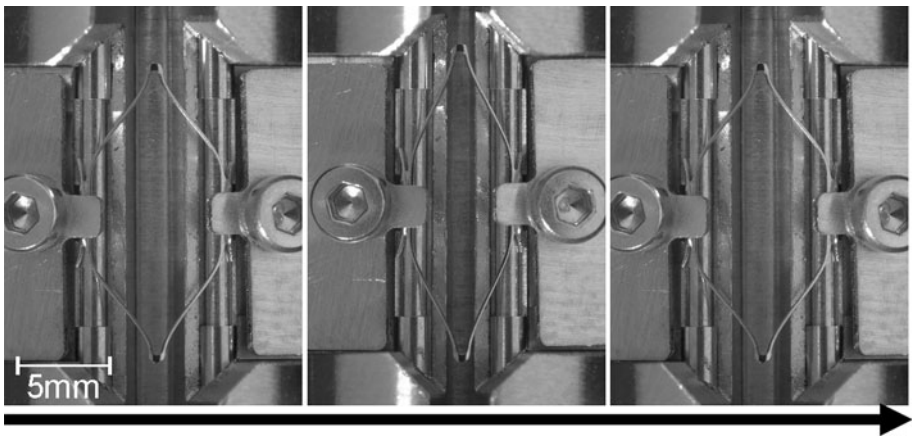

Fig. 3 Deformation of the diamond specimen in the specimen holder of the test rig

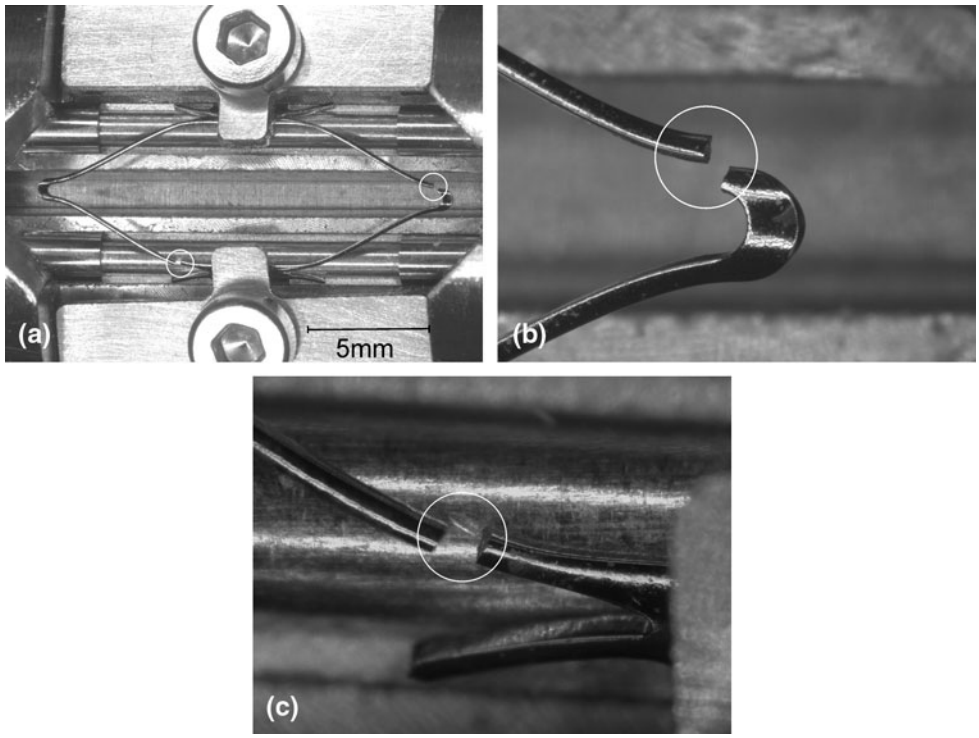

Fig. 4 Diamond test specimen with fractures (see circles) at the specimen apex (top right) and nearby clamping (bottom)

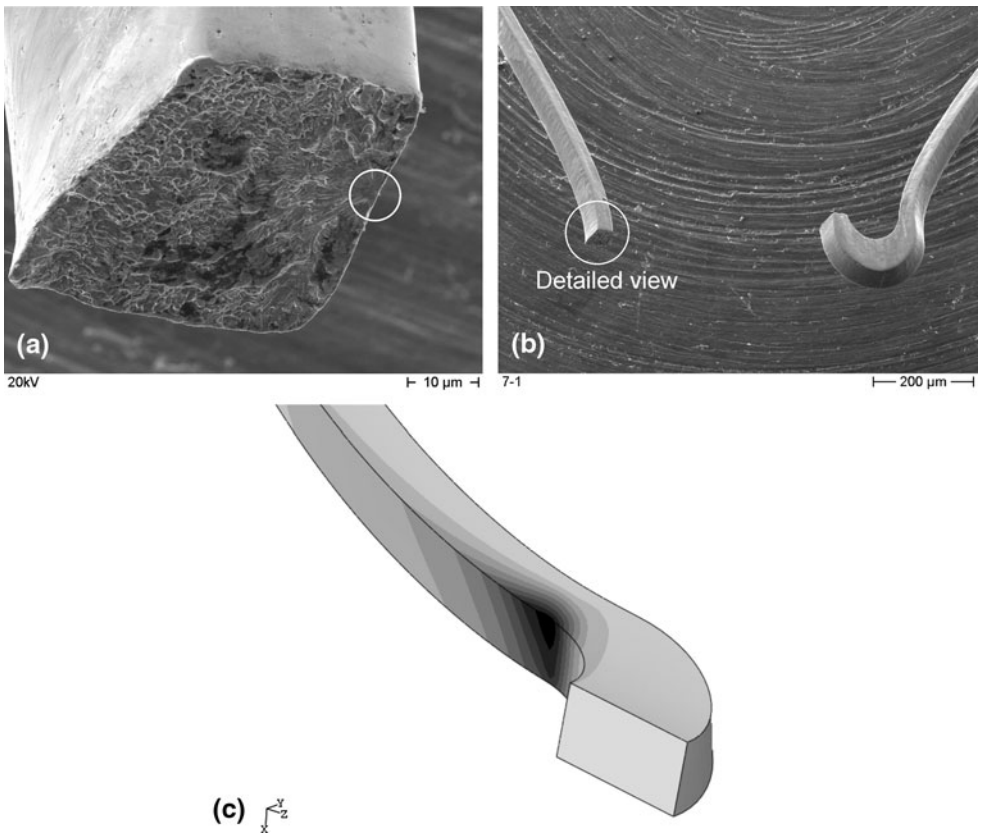

Fig. 5 SEM image of a fracture surface; FEA confirmed crack initiation corresponded to the location of maximum strain amplitude (darker color indicates higher strain levels). Crack initiation is marked with a circle

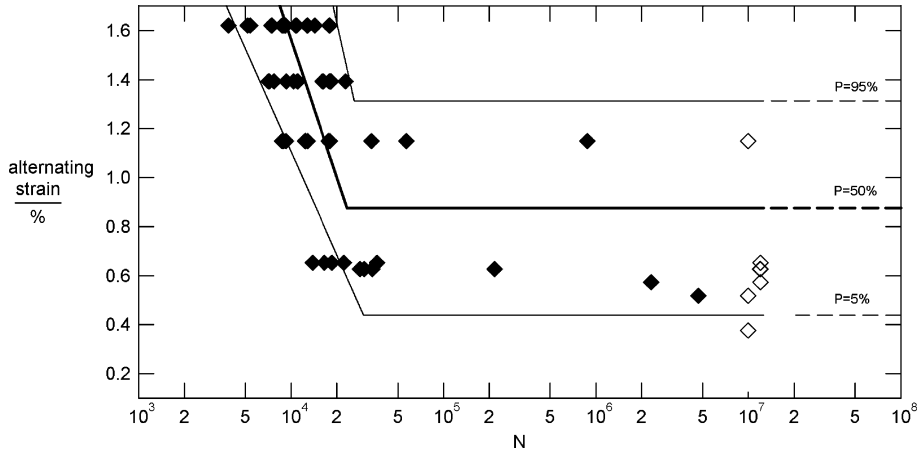

Fig. 6 Strain-cycle curve for the diamond specimen cycled to 10^7 cycles with regression lines for 5, 50, and 95% failure probability for a mean strain of approx. 2.5%

Table 1 Number of fractured specimens as well as run-outs for the individual strain levels

Strain level, %	No. of fractured specimens	No. of specimens survived (run-outs)	Comments
1.62	16	0	None
1.39	16	0	None
1.15	*13*	*3*	*None*
0.65	*5*	*11*	*None*
0.63	*5*	*11*	*None*
0.57	*1*	*15*	*None*
0.52	*1*	*14*	*One specimen has been excluded due to a mechanically pre-damaged strut caused by the cutting-off of the specimen*
0.38	0	16	None

Italics representations in the cells highlight the strain levels which show a bimodal distribution (fractures and run-outs)

inner radius of the specimen close to the middle of the strut height. The location of the crack initiation is under tension load.

Figure 6 shows the resulting strain-cycle curve for a mean strain of approx. 2.5% with regression lines for 5, 50, and 95% failure probability. The failure probabilities and strain-cycle curve have been determined with the help of commercially available software called SAFD (Ref 4). This software allows choosing between several estimation functions for the determination of the failure probabilities. The arc sine$\sqrt{P}$ transformation has been chosen for the graphical and mathematical evaluation for the ε/N curve since it is proved to be a technically appropriate model law for estimating fatigue strength and likewise minimum life. So far, this evaluation method worked very well at the field of fatigue data analysis that its application on a broad level is recommended (Ref 5-7). At strain amplitudes above 1.15% none of the specimens survived, while within a strain range of 0.52-1.15% a bimodal distribution occurred showing a consistent increase in fractures with increasing strain amplitude. All specimens survived at a strain amplitude of 0.38%. Table 1 shows the distribution of fractured specimens and specimens that survived for each strain level. The results indicate a failure probability of $P = 5\%$ for a strain amplitude of 0.44% (arc sine$\sqrt{P}$ transformation). The fractures were distributed near equally; there was less than a 5% greater chance of a fracture occurring at the apex than in the area adjacent to the clamping site.

4. Summary and Conclusions

This study investigated the fatigue behavior of stent-like diamond specimens with particular attention paid to the nature of the test specimen, the constitutive model for the finite element analyses and the displacement condition, realized by the development of a newly designed test rig, in order to enhance the study design and results. A failure probability of $P = 5\%$ was calculated for a strain amplitude of 0.44%. The existence of a relatively large range of strain that resulted in a bimodal distribution of both surviving and failing specimens could not be justified solely by the presence of inclusions, as crack initiation could not always be linked to the existence of an inclusion. The excellent performance of the new test method presented within this study provides a good basis for future tests without risk of compromised results due to differing characteristics between test specimens and finished stents, inappropriate loading conditions or constitutive material model and provides a high reliability and applicability of the results to actual stents.

Acknowledgments

The authors would like to thank Robert Boss for performing the tests and Rob Radford for conducting the finite element analyses. This study was conducted in the course of the work of a consortium of several stent manufacturers, SAFE Technology Limited, and Dassault Systèmes Simulia Corp., dedicated to the development of fatigue laws suitable for life prediction of Nitinol devices.

References

1. A.R. Pelton, X.-Y. Gong, and T. Duerig, Fatigue Testing of Diamond-Shaped Specimen, *SMST-2003: Proceedings of the Int. Conf. on Shape Memory and Superelastic Technologies*, A.R. Pelton and T. Duerig, Ed., Pacific Grove, CA, 2004, p 293–302
2. N.B. Morgan, J. Painter, and A. Moffat, Mean Strain Effects and Microstructural Observations During In vitro Fatigue Testing of NiTi, *SMST-2003: Proceedings of the Int. Conf. on Shape Memory and Superelastic Technologies*, A.R. Pelton and T. Duerig, Ed., Pacific Grove, CA, 2004, p 303–310
3. A. Wick, X.-Y. Gong, J. Fino, J. Sheriff, and A.R. Pelton, Bending Fatigue Characteristics of Nitinol, *SMST-2004: Proceedings of the Int. Conf. on Shape Memory and Superelastic Technologies*, M. Mertmann, Ed., Baden-Baden, Germany, 2006, p 89–94
4. SAFD, "Statistical Analysis of Fatigue Data," Version 5.5, Nov. 2006, RWTH Aachen
5. D. Dengel, Die arcsin √P-Transformation—ein einfaches Verfahren zur graphischen und rechnerischen Auswertung geplanter Wöhlerversuche, *Z. Werkstofftech.*, 1974, **6**, p 253–261
6. DIN 969, Ausgabe:1997-12,"Verbindungselemente mit Gewinde—Schwingfestigkeitsversuch bei Axialbelastung—Prüfverfahren und Auswertung der Ergebnisse"
7. ISO 3800:1993-(E), Threaded Fasteners—Axial Load Fatigue Testing—Test Methods and Evaluation of Results